Chemical Science

ROYAL SOCIETY OF CHEMISTRY

EDGE ARTICLE

Cite this: *Chem. Sci.*, 2020, **11**, 8176

All publication charges for this article have been paid for by the Royal Society of Chemistry

Isomerization-induced enhancement of luminescence in $Au_{28}(SR)_{20}$ nanoclusters†

Yuxiang Chen, Meng Zhou, Qi Li, Harrison Gronlund and Rongchao Jin *

Understanding the origin and structural basis of the photoluminescence (PL) phenomenon in thiolate-protected metal nanoclusters is of paramount importance for both fundamental science and practical applications. It remains a major challenge to correlate the PL properties with the atomic-level structure due to the complex interplay of the metal core (*i.e.* the inner kernel) and the exterior shell (*i.e.* surface Au(I)-thiolate staple motifs). Decoupling these two intertwined structural factors is critical in order to understand the PL origin. Herein, we utilize two $Au_{28}(SR)_{20}$ nanoclusters with different –R groups, which possess the same core but different shell structures and thus provide an ideal system for the PL study. We discover that the $Au_{28}(CHT)_{20}$ (CHT: cyclohexanethiolate) nanocluster exhibits a more than 15-fold higher PL quantum yield than the $Au_{28}(TBBT)_{20}$ nanocluster (TBBT: *p*-*tert*-butylbenzenethiolate). Such an enhancement is found to originate from the different structural arrangement of the staple motifs in the shell, which modifies the electron relaxation dynamics in the inner core to different extents for the two nanoclusters. The emergence of a long PL lifetime component in the more emissive $Au_{28}(CHT)_{20}$ nanocluster reveals that its PL is enhanced by suppressing the nonradiative pathway. The presence of long, interlocked staple motifs is further identified as a key structural parameter that favors the luminescence. Overall, this work offers structural insights into the PL origin in $Au_{28}(SR)_{20}$ nanoclusters and provides some guidelines for designing luminescent metal nanoclusters for sensing and optoelectronic applications.

Received 28th February 2020
Accepted 16th July 2020

DOI: 10.1039/d0sc01270j

rsc.li/chemical-science

Introduction

Atomically precise metal nanoclusters have emerged as a new class of nanomaterials in recent years and hold promise in many applications such as chemical sensing, biological imaging, and catalysis.[1–12] Luminescent metal nanoclusters are of particular interest owing to their unique properties, including their high stability, low toxicity, large Stokes shift, and long luminescence lifetime, and thus such nanoclusters have attracted significant research interest in recent years.[13–24]

A major effort in current research on luminescent nanoclusters protected by thiolates is focused on the development of effective strategies to enhance their luminescence. To improve the quantum yield of photoluminescence (PL), it is of paramount importance to understand the PL mechanism and, in particular, the structural basis.[18] Toward this goal, significant efforts have been made in recent years.[25–37] Wu *et al.* identified that the presence of electron-rich atoms (*e.g.*, oxygen and nitrogen) or functional groups (*e.g.*, the carboxyl or amine group) in the thiolate ligands could enhance the PL of $Au_{25}(SR)_{18}$ nanoclusters *via* ligand to metal core charge transfer.[25] Xie *et al.* reported an aggregation induced emission (AIE) mechanism in gold nanoclusters.[28–30] Lee *et al.* reported that rigidifying the gold shell of the nanocluster can efficiently enhance PL.[31] Foreign metal doping and alloying is also an important strategy for boosting the PL in metal nanoclusters.[37–40] Theoretical insights into PL have been obtained by Aikens *et al.*[26] Despite such progress, atomic-level understanding of the origin and structural basis for the PL mechanism in metal nanoclusters still remains a challenge.

Intense research on gold nanoclusters have created a series of atomically precise nanoclusters with diverse and tunable structures.[1,41–49] For example, by utilizing ligand-based synthetic strategies, atomic-level control has been achieved in manipulating the cluster size,[50] shape[51] (such as hexagonal prism shaped Au_{40} *vs.* tetragonal rod shaped Au_{52}), surface structure,[43,52] and core structure.[53–55] With the valuable structural information, it has become possible to precisely correlate the PL properties of gold nanoclusters with the atomic structure.[33]

For thiolate-protected $Au_n(SR)_m$ nanoclusters, both the inner gold kernel (hereafter referred to as *core*) and surface $Au_x(SR)_{x+1}$ motifs (hereafter referred to as *shell*) are considered as important contributors to their PL properties.[28,56] For the well-studied icosahedral $Au_{25}(SR)_{18}$ nanocluster, the core-to-shell relaxation

Department of Chemistry, Carnegie Mellon University, Pennsylvania 15213, USA. E-mail: rongchao@andrew.cmu.edu

† Electronic supplementary information (ESI) available. See DOI: 10.1039/d0sc01270j

was observed in ultrafast electron dynamics and the PL mechanism was interpreted,[57–61] including the theoretical insights.[35] However, the PL origin and mechanism for other $Au_n(SR)_m$ nanoclusters with non-icosahedral structures largely remain unclear, albeit all possess the core–shell structures. In consideration of the coupling between the core and the shell, the individual roles of these two intertwined structural parameters have not been elucidated. Thus, an important step toward atomic-level understanding of PL is to decouple these two structural parts by selectively changing one while retaining the other and then investigate the effect to identify the mechanistic pathway. The 28-gold-atom nanocluster,[52] *i.e.*, $Au_{28}(CHT)_{20}$ (CHT = cyclohexanethiolate) and $Au_{28}(TBBT)_{20}$ (TBBT = *p-tert*-butylbenzenethiolate), which share the same core but different shell structures, can serve as an ideal system for such a purpose.

Herein, the luminescence origin of the two $Au_{28}(SR)_{20}$ nanoclusters is investigated. Interestingly, the $Au_{28}(CHT)_{20}$ nanocluster exhibits more than 15-fold higher PL quantum yield than $Au_{28}(TBBT)_{20}$. Time-resolved PL measurements identify a long lifetime component in $Au_{28}(CHT)_{20}$, indicating that the nonradiative pathway is suppressed compared to that in $Au_{28}(TBBT)_{20}$. To understand the enhancement of PL, ultrafast transient absorption spectroscopy is employed to probe the electron dynamics of these two correlated nanoclusters. Based on all the results, we present a shell-mediated core emission mechanism to explain the structural origin of the PL in $Au_{28}(SR)_{20}$ nanoclusters. In such a luminescence pathway, the emission solely arises from the metal core while the electron dynamics of the core is distinctly influenced by the shell.

Results and discussion

The synthesis of the $Au_{28}(TBBT)_{20}$ nanocluster followed a previously reported approach,[49] and the $Au_{28}(CHT)_{20}$ was obtained by a ligand-induced isomerization reaction of $Au_{28}(TBBT)_{20}$ with excess cyclohexanethiol at 80 °C.[52] Both $Au_{28}(SR)_{20}$ nanoclusters are thermally robust and their total structures were determined by X-ray crystallography[49,52] as shown in Fig. 1. The $Au_{28}(CHT)_{20}$ and $Au_{28}(TBBT)_{20}$ nanoclusters have the same inner Au_{14} core structure (Fig. 1a and d) but distinctly different shell structures (*i.e.*, surface staple motifs, Fig. 1b and e). It is worth noting that, for face-centered cubic (FCC) gold nanoclusters, there are several alternative ways to categorize the core and shell gold atoms.[62] Here we consider the gold atoms with the shortest Au–Au bond lengths (*i.e.*, average 2.83 Å in $Au_{28}(CHT)_{20}$ and 2.84 Å in $Au_{28}(TBBT)_{20}$) as the core (Fig. 1a and d). In this view, both $Au_{28}(SR)_{20}$ isomers have the same Au_{14} core, which consists of a dimer of bitetrahedral Au_7. The Au_7 unit can further be dissected into two Au_4 units that share one common vertex (see the ESI, Fig. S1†). This view of the core structure is supported by X-ray absorption spectroscopy,[63] Bader charge analysis,[64] and other theoretical analyses.[65–67] Of note, other views (*e.g.*, cuboctahedron or a cubic box)[52,62] do not affect the fact that the two $Au_{28}(SR)_{20}$ nanoclusters have the same gold core but different shells.

The shell structure exhibits completely different arrangements between the two $Au_{28}(SR)_{20}$ nanoclusters. In the $Au_{28}(CHT)_{20}$ nanocluster, the Au_{14} core is surrounded by two monomeric staple motifs (SR-Au-SR) and four trimeric staple

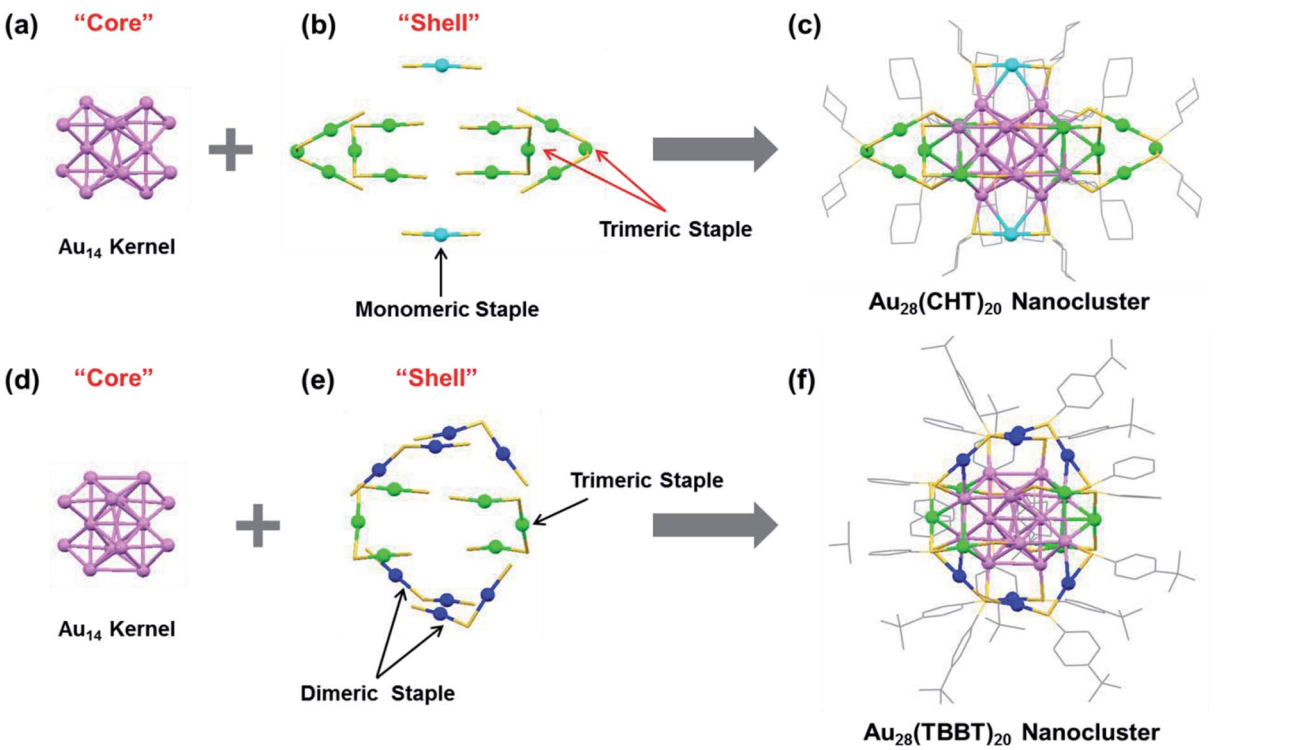

Fig. 1 X-ray structures of (a–c) $Au_{28}(CHT)_{20}$ and (d–f) $Au_{28}(TBBT)_{20}$ featuring the "core" and "shell" components. Color labels: purple = core Au atoms; other colors = shell Au atoms. The carbon tails in (b and e) are omitted for clarity. Redrawn from ref. 49 and 52.

motifs (SR-Au-SR-Au-SR-Au-SR), Fig. 1b. The trimeric motifs form two pairs of interlocked configuration (highlighted with red arrows in Fig. 1b). In contrast, the shell of $Au_{28}(TBBT)_{20}$ contains four dimeric staples (SR-Au-SR-Au-SR) and two trimeric staples (SR-Au-SR-Au-SR-Au-SR), Fig. 1e. The total structures of $Au_{28}(CHT)_{20}$ and $Au_{28}(TBBT)_{20}$ are shown in Fig. 1c and f. The two $Au_{28}(SR)_{20}$ nanoclusters motivate us to investigate their PL properties in the current work.

The optical absorption spectra of the $Au_{28}(CHT)_{20}$ and $Au_{28}(TBBT)_{20}$ nanoclusters are shown in Fig. 2a and c, respectively. Both $Au_{28}(SR)_{20}$ nanoclusters exhibit very similar UV-vis optical features despite the blue shifting of the absorption bands for $Au_{28}(CHT)_{20}$ compared with those of $Au_{28}(TBBT)_{20}$. It is worth noting that these two $Au_{28}(SR)_{20}$ isomers also exhibit a similar HOMO–LUMO band gap around 1.7 eV as determined from their optical spectra and differential pulse voltammogram.[68] The closely resembling optical absorption spectra indicate that the core structure dictates the absorption spectra.

The photo excitation and emission spectra of $Au_{28}(CHT)_{20}$ and $Au_{28}(TBBT)_{20}$ are shown in Fig. 2b and d, respectively. The PL emission spectrum of $Au_{28}(CHT)_{20}$ is centered at ~784 nm (Fig. 2b, red profile). The PL excitation spectrum exhibits three peaks with the highest peak at 372 nm (Fig. 2b, blue profile). For $Au_{28}(TBBT)_{20}$, the PL spectrum is centered at 756 nm which is blue shifted compared with $Au_{28}(CHT)_{20}$ (Fig. 2d). The PL excitation spectrum of $Au_{28}(TBBT)_{20}$ also shows three bands but less distinct, in comparison to $Au_{28}(CHT)_{20}$ (Fig. 2d). Interestingly, the PL intensity of $Au_{28}(CHT)_{20}$ is significantly higher than that of $Au_{28}(TBBT)_{20}$ as revealed in the excitation/emission contour maps (Fig. 3a and b). The PL excitation was scanned from 300 to 700 nm and the emission profile was recorded from 600 to 900 nm. As shown in Fig. 3, although both $Au_{28}(SR)_{20}$ nanoclusters emit in the 725 to 825 nm region, the quantum yield (QY) of $Au_{28}(CHT)_{20}$ is more than 15-fold higher than that of $Au_{28}(TBBT)_{20}$, *i.e.* 1.6% *vs.* 0.1%. Herein, the QY measurements used $Au_{25}(SG)_{18}$ (QY = 0.2%)[25] as the reference. We note that gold nanoclusters protected by *hydrophobic* thiolates are often weak in luminescence (QY < 1%). Only a few gold nanoclusters, *i.e.*, the present $Au_{28}(CHT)_{20}$ and the previously reported $Au_{24}(SR)_{20}$ (R = CH_2Ph-^{t}Bu, CH_2Ph, C_2H_4Ph) have QYs greater than 1%.[15,16,27]

To gain insight into the luminescence behavior of the two nanoclusters, the PL lifetime was measured by time-correlated single photon counting (TCSPC). As shown in Fig. 4, multi-exponential fitting of the PL decay profiles gives rise to two lifetime components for each nanocluster, *i.e.*, τ_1 = 264 ns (25%) and τ_2 = 1.70 μs (75%) for $Au_{28}(CHT)_{20}$, and τ_1 = 59 ns (56%) and τ_2 = 285 ns (44%) for $Au_{28}(TBBT)_{20}$. It is clear that $Au_{28}(CHT)_{20}$ exhibits a significantly longer PL lifetime than $Au_{28}(TBBT)_{20}$ (Fig. 4). The long-lived component explains the higher QY of $Au_{28}(CHT)_{20}$. The average lifetime (τ*) and QY are related by eqn (1),

$$QY = \tau^* k_R \quad (1)$$

where k_R is the radiative decay rate. The average lifetime (τ*) can be calculated using eqn (2),

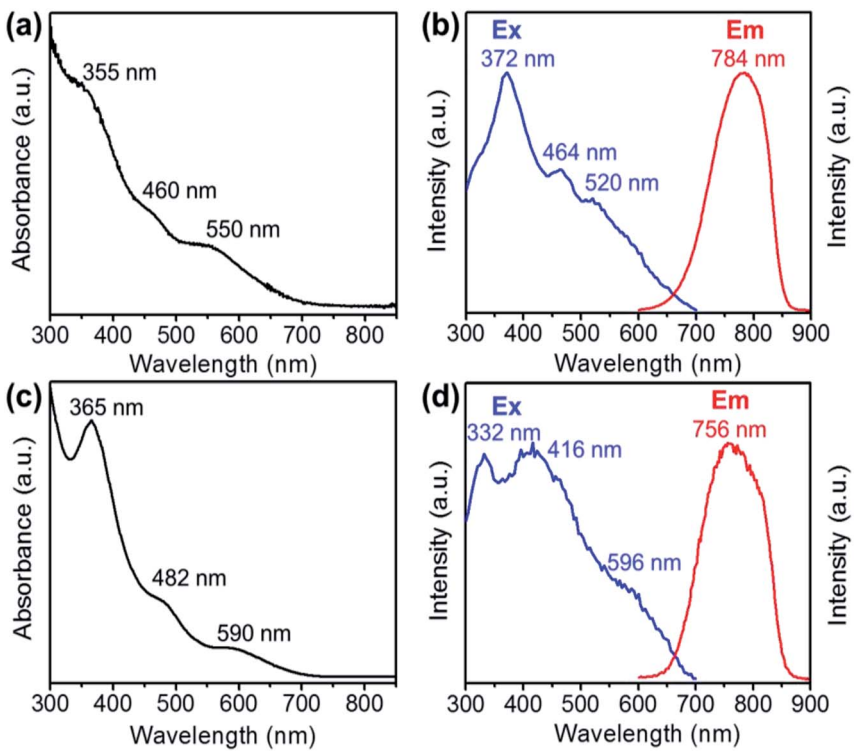

Fig. 2 UV-vis absorption spectra of (a) $Au_{28}(CHT)_{20}$ and (c) $Au_{28}(TBBT)_{20}$. Photoluminescence excitation (Ex, monitored emission at the maximum intensity) and emission (Em, excited at 372 nm) spectra of (b) $Au_{28}(CHT)_{20}$ and (d) $Au_{28}(TBBT)_{20}$.

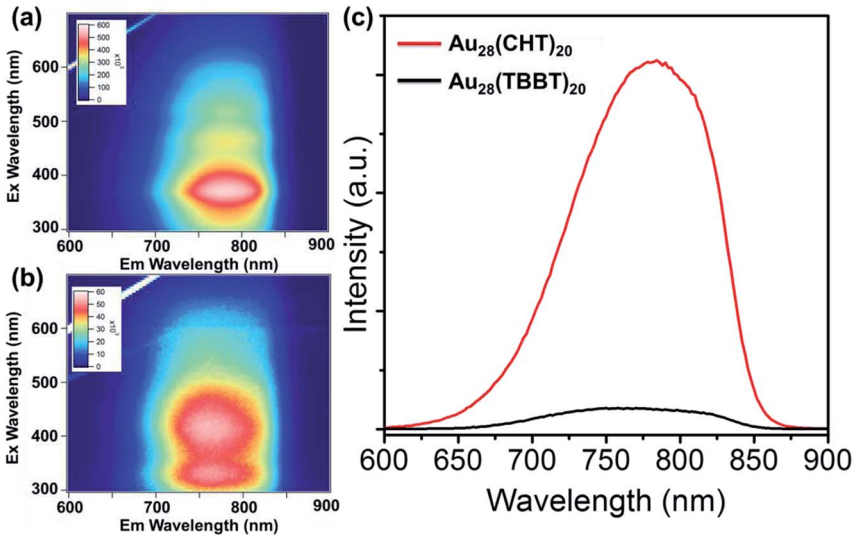

Fig. 3 Excitation/emission contour maps of (a) $Au_{28}(CHT)_{20}$ and (b) $Au_{28}(TBBT)_{20}$. (c) Comparison of the emission spectra of $Au_{28}(CHT)_{20}$ and $Au_{28}(TBBT)_{20}$ excited at 372 nm.

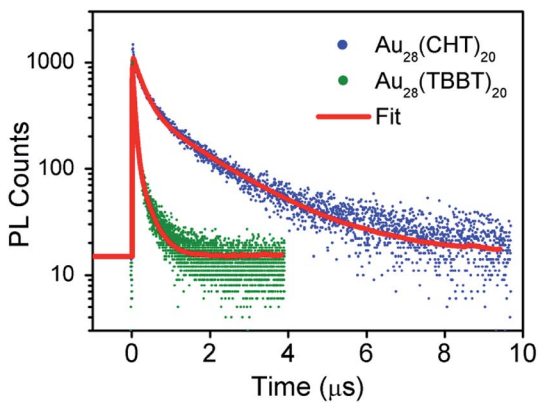

Fig. 4 Comparison of the photoluminescence decays of $Au_{28}(CHT)_{20}$ and $Au_{28}(TBBT)_{20}$ nanoclusters at the emission maxima measured by TCSPC.

$$\tau^* = \frac{\sum_i A_i \tau_i}{\sum_i A_i} \quad (2)$$

where A_i is the relative amplitude and τ_i is the individual i^{th} lifetime. Therefore, the radiative decay rate (k_R) can be obtained. With the experimentally measured QY and calculated k_R, the non-radiative decay rate (k_{NR}) can also be obtained according to the relation shown in eqn (3).

$$QY = \frac{k_R}{k_R + k_{NR}} \quad (3)$$

The measured and calculated parameters are summarized in Table 1.

Generally, PL can be increased by (i) enhancing the radiative rate (accordingly, the PL lifetime becomes shorter), and/or (ii) suppressing the nonradiative rate (accordingly, the PL lifetime becomes longer). In our system, apparently the PL enhancement in $Au_{28}(CHT)_{20}$ falls in the second category since the lifetime becomes much longer. The mechanism for suppressing the non-radiative decay rate (k_{NR}) in the $Au_{28}(CHT)_{20}$ nanocluster is further discussed below.

To further understand the origin of the difference in the PL intensity and lifetime for the two $Au_{28}(SR)_{20}$ nanoclusters, femtosecond and nanosecond transient absorption (TA) spectroscopy measurements were performed to probe the detailed excited state relaxation and dynamics. As shown in Fig. 5a and b, the two $Au_{28}(SR)_{20}$ isomers exhibit very similar TA spectra at $\Delta t = 1$ ns. The excited state absorption (ESA) overlaps with ground state bleaching (GSB) in both $Au_{28}(SR)_{20}$ isomers. All the GSB and ESA peaks of $Au_{28}(CHT)_{20}$ are blue-shifted compared with those of $Au_{28}(TBBT)_{20}$, which agrees well with the trend in their steady-state absorption spectra (Fig. 2a and c). Significantly, despite the two nanoclusters having similar TA spectra, drastic differences were observed in their excited state lifetimes (Fig. 5c and d), that is, the ESA of $Au_{28}(TBBT)_{20}$ decays to zero within ~300 ns while the decay of ESA in $Au_{28}(CHT)_{20}$ at a similar probe wavelength takes a significantly longer time (~10 μs). Global fitting shows that the excited state lifetime of $Au_{28}(CHT)_{20}$ has three components (8 ns, 105 ns and 1.7 μs), while $Au_{28}(TBBT)_{20}$ shows two components (58 ns and 200 ns). The significantly longer excited state lifetime of $Au_{28}(CHT)_{20}$

Table 1 Parameters obtained from photoluminescence measurements[a]

	QY (%)	τ^*	k_R (s^{-1})	k_{NR} (s^{-1})
$Au_{28}(CHT)_{20}$	1.6	1341 ns	1.19×10^4	7.32×10^5
$Au_{28}(TBBT)_{20}$	0.1	158 ns	6.33×10^3	6.32×10^6

[a] QY: quantum yield, τ^*: average lifetime, k_R: radiative decay rate, k_{NR}: non-radiative decay rate.

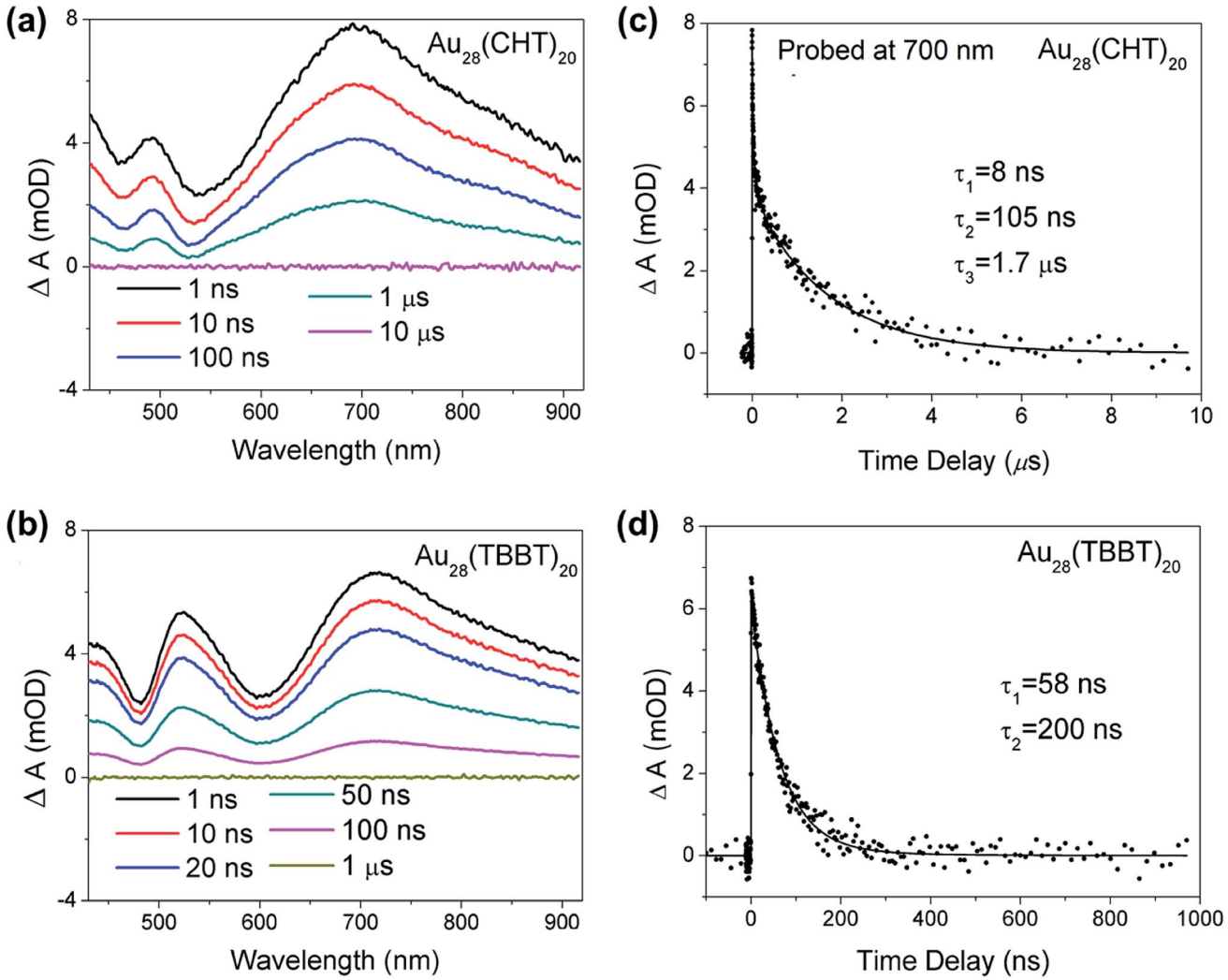

Fig. 5 Nanosecond transient absorption spectra of (a) $Au_{28}(CHT)_{20}$ and (b) $Au_{28}(TBBT)_{20}$ at selected time delays pumped at 360 nm. Kinetic traces probed at 700 nm for (c) $Au_{28}(CHT)_{20}$ and (d) $Au_{28}(TBBT)_{20}$. The corresponding fits are obtained from global fitting.

from TA measurements is in line with the PL lifetime results measured by TCSPC, which further supports that the long-lived excited state is responsible for the stronger PL in the $Au_{28}(CHT)_{20}$ nanocluster, that is, the PL enhancement mechanism is *via* suppressing the nonradiative rate, as opposed to enhancing the radiative rate. The resemblance of the excited state lifetimes measured by nanosecond TA spectroscopy and the TCSPC explicitly indicates that the TA and PL signals have a similar geometrical and electronic origin.

In addition to the above nanosecond dynamics, femtosecond transient absorption measurements with a pump at 600 nm (near-bandgap excitation) were also carried out to probe the ultrafast electron dynamics of the two $Au_{28}(SR)_{20}$ nanoclusters. Interestingly, both $Au_{28}(SR)_{20}$ nanoclusters did not exhibit any ~1 ps component that corresponds to the core–shell relaxation observed in a $Au_{25}(SR)_{18}$ nanocluster.[57–59] Since no additional spectral features with near-bandgap excitation was observed (Fig. 6), we conclude that there is no core-to-shell electron transfer (or core–shell relaxation) in both $Au_{28}(SR)_{20}$ nanoclusters. As shown in Fig. 6, both $Au_{28}(SR)_{20}$ nanoclusters exhibit picosecond and nanosecond decaying components with similar evolution associated spectral (EAS) features. Therefore, the picosecond relaxation can be attributed to the structural relaxation.[69] These results are distinctly different from the core–shell relaxation mode previously observed in $Au_{25}(SR)_{18}$ and $Au_{38}(SR)_{24}$ nanoclusters.[57–59,69]

Based on the femtosecond and nanosecond transient absorption measurements, the relaxation pathway for both $Au_{28}(SR)_{20}$ isomers is summarized in Scheme 1 with respective time constants. Such a relaxation pathway is completely different from the previously observed two-state relaxation for $Au_{25}(SR)_{18}$ and $Au_{38}(SR)_{24}$ nanoclusters.[59,60,69] The absence of core–shell electronic relaxation in both $Au_{28}(SR)_{20}$ nanoclusters suggests that the electrons are mostly localized in the metal core where the TA signals originated. Therefore, the inner metal core is the key and constitutes the structural origin for the distinct differences in the PL intensity and excited state lifetime between the two $Au_{28}(SR)_{20}$ nanoclusters. As both $Au_{28}(SR)_{20}$ nanoclusters have the same Au_{14} core (note: the Au–Au bond length difference between the two Au_{14} cores is less than 0.4%),

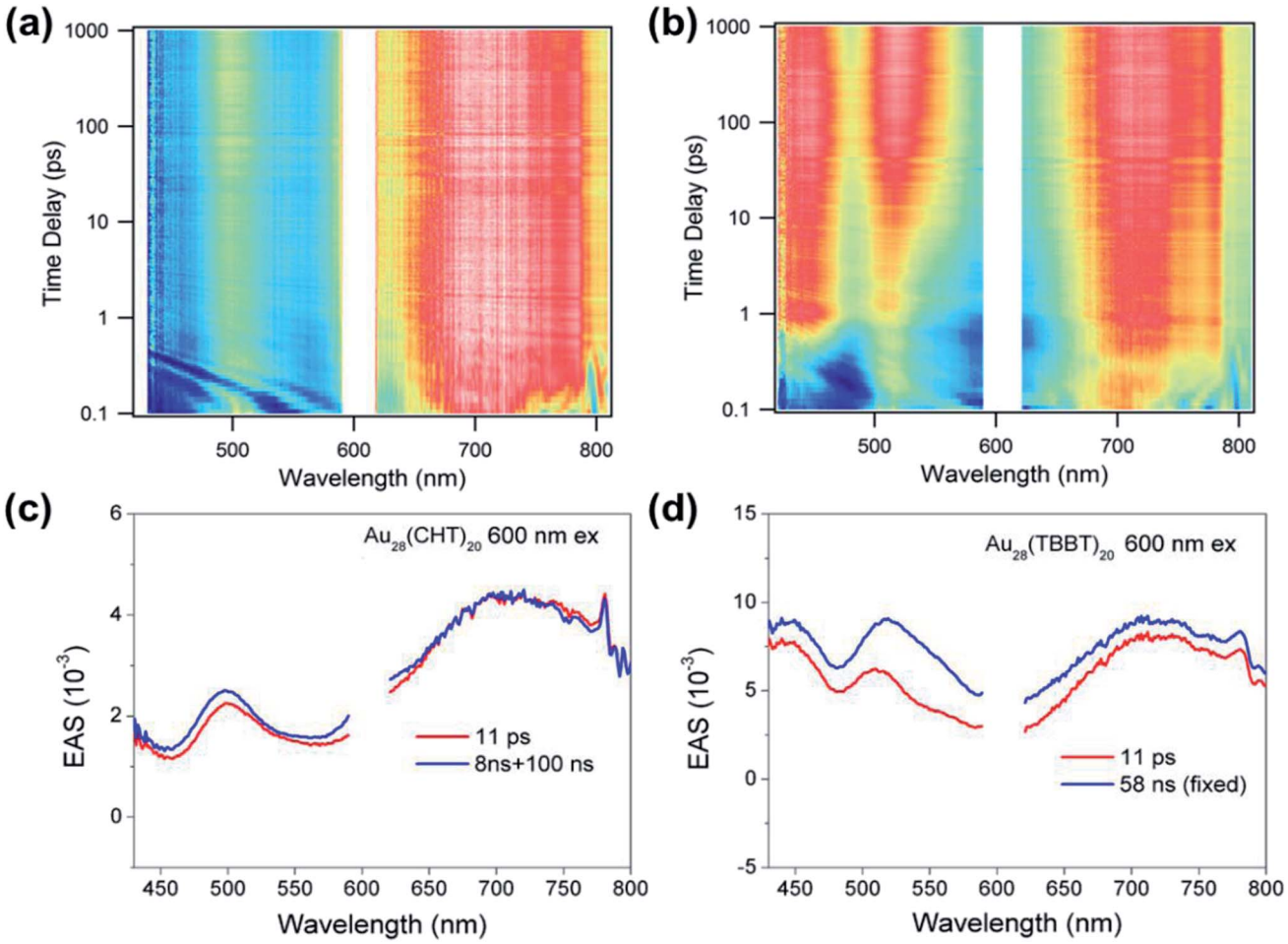

Fig. 6 Femtosecond transient absorption data map of (a) $Au_{28}(TBBT)_{20}$ and (b) $Au_{28}(CHT)_{20}$ pumped at 600 nm. Evolution associated spectra (EAS) obtained from global fitting of (c) $Au_{28}(TBBT)_{20}$ and (d) $Au_{28}(CHT)_{20}$. Note: scattering around 600 nm due to the pump pulse was cut off in both $Au_{28}(SR)_{20}$ nanoclusters.

we conclude that the shell structures heavily influence or even dictate the electronic relaxation and dynamics of the metal core, which indirectly affects the PL properties. These results suggest that the PL originated from the metal core, instead of the shell.

Based on the above results, we propose a shell-mediated core emission mechanism to explain the structural origin of the PL in the $Au_{28}(SR)_{20}$ nanoclusters. In such a luminescence pathway, the emission solely arises from the metal core while the electron dynamics of the core is modulated by the shell. This core-originated PL mechanism in $Au_{28}(SR)_{20}$ nanoclusters is quite unique, and it is distinctly different from the previously observed surface-initiated emission behavior for $Au_{25}(SR)_{18}$ and

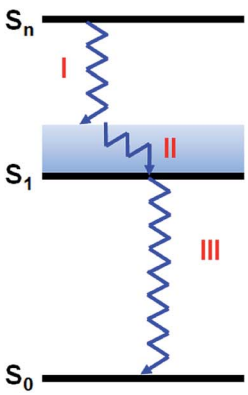

	$Au_{28}(CHT)_{20}$	$Au_{28}(TBBT)_{20}$
I	100-200 fs	100-200 fs
II	11 ps	11 ps
III	8ns, 105 ns 1.7 μs	58 ns, 200 ns

I: Internal Conversion II: Core Relaxation III: $S_1 \rightarrow S_0$

Scheme 1 Relaxation diagram of $Au_{28}(SR)_{20}$ nanoclusters and time constants obtained from transient absorption measurements.

other water soluble glutathione (SG)-protected gold nanoclusters.[19,25] Such a different origin of PL (*i.e.*, core *vs.* surface) is attributed to the unique Au_4-assembled or FCC core structure in $Au_{28}(SR)_{20}$ nanoclusters as opposed to the icosahedron-based structures in $Au_{25}(SR)_{18}$ and other related nanoclusters. This core-originated emission may also exist in other FCC based gold nanoclusters. Other than the core-originated PL, the 15-fold enhancement in $Au_{28}(CHT)_{20}$ compared to $Au_{28}(TBBT)_{20}$ implies that the shell structure also plays an important role, which is due to the electronic interactions between the core and the shell.

Finally, it is worth noting that Au(I)-SR complexes[70] and polymers[71] could be luminescent. Thus, we prepared[72] and tested both Au(I)CHT and Au(I)TBBT for PL, but no appreciable PL was found (see the ESI, Fig. S2†). Upon correlating with the X-ray structures of $Au_{28}(CHT)_{20}$ and $Au_{28}(TBBT)_{20}$, one can find that, in $Au_{28}(CHT)_{20}$, the staples are quite dangling out, which leads to less interactions with the kernel and thus slower excitation energy dumping through the surface (to solvent), whereas the $Au_{28}(TBBT)_{20}$ has a tighter interaction between staples and the kernel, which leads to faster dumping of electronic excitation energy. The interlocking of staple motifs also enhances the PL owing to surface rigidification. In summary, given the structure-dependence of PL, the origins of PL in metal nanoclusters are most probably multi-fold (*e.g.* FCC-related origin *vs.* icosahedral structure origin), and future work is expected to map out more mechanisms through structure-PL correlations.

Conclusion

Using the pair of $Au_{28}(CHT)_{20}$ and $Au_{28}(TBBT)_{20}$ nanoclusters as a model system, we have investigated the photoluminescence origin. Interestingly, we find that the QY of the $Au_{28}(CHT)_{20}$ nanocluster is more than 15-fold higher than that of $Au_{28}(TBBT)_{20}$. Correlating the PL and the excited state electron dynamics with the atomic structures of the two $Au_{28}(SR)_{20}$ nanoclusters reveals a shell-mediated core emission mechanism. The discovery of the core-originated emission mechanism in FCC based $Au_{28}(SR)_{20}$ nanoclusters is significant since it provides new insights into the intriguing PL phenomenon in non-icosahedral gold nanoclusters. The present study offers important guidelines for rationally enhancing the luminescence of metal nanoclusters for various applications.

Conflicts of interest

There are no conflicts to declare.

Acknowledgements

We thank Dr Yongbo Song for assistance with the preparation and PL measurements of Au(I)CHT and Au(I)TBBT complexes. R. J. acknowledges financial support by the Air Force Office of Scientific Research and the U.S. National Science Foundation (DMR-1808675).

References

1 M. Zhou, T. Higaki, G. Hu, M. Y. Sfeir, Y. Chen, D. Jiang and R. Jin, *Science*, 2019, **364**, 279–282.
2 Z. J. Guan, F. Hu, S. F. Yuan, A. A. Nan, Y. M Lin and Q.-M. Wang, *Chem. Sci.*, 2019, **10**, 3360–3365.
3 M. Yu, J. Zhou, B. Du, X. Ning, C. Authement, L. Gandee, P. Kapur, J. T. Hsieh and J. Zheng, *Angew. Chem., Int. Ed.*, 2016, **55**, 2787–2791.
4 Y. Z. Li, R. Ganguly, K. Y. Hong, Y. Li, M. E. Tessensohn, R. Webster and W. K. Leong, *Chem. Sci.*, 2018, **9**, 8723–8730.
5 X. Yuan, Z. Luo, Y. Yu, Q. Yao and J. Xie, *Chem.–Asian J.*, 2013, **8**, 858–871.
6 L.-Y. Chen, C.-W. Wang, Z. Yuan and H.-T. Chang, *Anal. Chem.*, 2015, **87**, 216–229.
7 A. W. Cook and T. W. Hayton, *Acc. Chem. Res.*, 2018, **51**, 2456–2464.
8 Y. Chen, M. L. Phipps, J. H. Werner, S. Chakraborty and J. S. Martinez, *Acc. Chem. Res.*, 2018, **51**, 2756–2763.
9 K. K. Chakrahari, R. P. B. Silalahi, J. H. Liao, S. Kahlal, Y. C. Liu, J. F. Lee, M. H. Chiang, J. Y. Saillard and C. W. Liu, *Chem. Sci.*, 2018, **9**, 6785–6795.
10 Y. M. Su, Z. Wang, G. L. Zhuang, Q. Q. Zhao, Z. P. Wang, C. H. Tung and D. Sun, *Chem. Sci.*, 2019, **10**, 564–568.
11 P. L. Xavier, K. Chaudhari, A. Baksi and T. Pradeep, *Nano Rev.*, 2012, **3**, 14767.
12 X.-K. Wan, W. W. Xu, S.-F. Yuan, Y. Gao, X.-C. Zeng and Q.-M. Wang, *Angew. Chem., Int. Ed.*, 2015, **127**, 9819–9822.
13 Y. Yu, Z. Luo, D. M. Chevrier, D. T. Leong, P. Zhang, D.-e. Jiang and J. Xie, *J. Am. Chem. Soc.*, 2014, **136**, 1246–1249.
14 X. Kang, S. Wang and M. Zhu, *Chem. Sci.*, 2018, **9**, 3062–3068.
15 A. Das, T. Li, G. Li, K. Nobusada, C. Zeng, N. L. Rosi and R. Jin, *Nanoscale*, 2014, **6**, 6458–6462.
16 C. Yao, S. Tian, L. Liao, X. Liu, N. Xia, N. Yan, Z. Gan and Z. Wu, *Nanoscale*, 2015, **7**, 16200–16203.
17 Z. Tang, T. Ahuja, S. Wang and G. Wang, *Nanoscale*, 2012, **4**, 4119–4124.
18 J. Liu, P. N. Duchesne, M. Yu, X. Jiang, X. Ning, R. D. Vinluan III, P. Zhang and J. Zheng, *Angew. Chem., Int. Ed.*, 2016, **55**, 8894–8898.
19 Y. Negishi, K. Nobusada and T. Tsukuda, *J. Am. Chem. Soc.*, 2005, **127**, 5261–5270.
20 D. M. Chevrier, V. D. Thanthirige, Z. Luo, S. Driscoll, P. Cho, M. A. MacDonald, Q. Yao, R. Guda, J. Xie, E. R. Johnson, A. Chatt, N. Zheng and P. Zhang, *Chem. Sci.*, 2018, **9**, 2782–2790.
21 K. Pyo, V. D. Thanthirige, S. Y. Yoon, G. Ramakrishna and D. Lee, *Nanoscale*, 2016, **8**, 20008–20016.
22 L. L. M. Zhang, G. Zhou, G. Zhou, H. K. Lee, N. Zhao, O. V. Prezhdo and T. C. W. Mak, *Chem. Sci.*, 2019, **10**, 10122–10128.
23 J. Jiang, C. V. Conroy, M. M. Kvetny, G. J. Lake, J. W. Padelford, T. Ahuja and G. Wang, *J. Phys. Chem. C*, 2014, **118**, 20680–20687.
24 Y.-T. Tseng, R. Cherng, S. G. Harroun, Z. Yuan, T.-Y. Lin, C.-W. Wu, H.-T. Chang and C.-C. Huang, *Nanoscale*, 2016, **8**, 9771–9779.

25 Z. Wu and R. Jin, *Nano Lett.*, 2010, **10**, 2568–2573.
26 C. M. Aikens, *Acc. Chem. Res.*, 2018, **51**, 3065–3073.
27 Z. Gan, Y. Lin, L. Luo, G. Han, W. Liu, Z. Liu, C. Yao, L. Weng, L. Liao, J. Chen, X. Liu, Y. Luo, C. Wang, S. Wei and Z. Wu, *Angew. Chem., Int. Ed.*, 2016, **55**, 11567–11571.
28 N. Goswami, Q. Yao, Z. Luo, J. Li, T. Chen and J. Xie, *J. Phys. Chem. Lett.*, 2016, **7**, 962–975.
29 Q. Yao, X. Yuan, T. Chen, D. T. Leong and J. Xie, *Adv. Mater.*, 2018, **30**, 1802751.
30 X. Dou, X. Yuan, Y. Yu, Z. Luo, Q. Yao, D. T. Leong and J. Xie, *Nanoscale*, 2014, **6**, 157–161.
31 K. Pyo, V. D. Thanthirige, K. Kwak, P. Pandurangan, G. Ramakrishna and D. Lee, *J. Am. Chem. Soc.*, 2015, **137**, 8244–8250.
32 L. G. AbdulHalim, M. S. Bootharaju, Q. Tang, S. del Gobbo, R. G. AbdulHalim, M. Eddaoudi, D.-e. Jiang and O. M. Bakr, *J. Am. Chem. Soc.*, 2015, **137**, 11970–11975.
33 K. L. D. M. Weerawardene, P. Pandeya, M. Zhou, Y. Chen, R. Jin and C. M. Aikens, *J. Am. Chem. Soc.*, 2019, **141**, 18715–18726.
34 X. Kang, S. Wang, Y. Song, S. Jin, G. Sun, H. Yu and M. Zhu, *Angew. Chem., Int. Ed.*, 2016, **55**, 3611–3614.
35 K. L. D. M. Weerawardene and C. M. Aikens, *J. Am. Chem. Soc.*, 2016, **138**, 11202–11210.
36 K. G. Stamplecoskie, Y.-S. Chen and P. V. Kamat, *J. Phys. Chem. C*, 2014, **118**, 1370–1376.
37 X. Kang, X. Wei, S. Jin, Q. Yuan, X. Luan, Y. Pei, S. Wang, M. Zhu and R. Jin, *Proc. Natl. Acad. Sci. U. S. A.*, 2019, **116**, 18834–18840.
38 S. Wang, X. Meng, A. Das, T. Li, Y. Song, T. Cao, X. Zhu, M. Zhu and R. Jin, *Angew. Chem., Int. Ed.*, 2014, **53**, 2376–2380.
39 G. Soldan, M. A. Aljuhani, M. S. Bootharaju, L. G. AbdulHalim, M. R. Parida, A.-H. Emwas, O. F. Mohammed and O. M. Bakr, *Angew. Chem., Int. Ed.*, 2016, **55**, 5749–5753.
40 M. S. Bootharaju, C. P. Joshi, M. R. Parida, O. F. Mohammed and O. M. Bakr, *Angew. Chem., Int. Ed.*, 2016, **55**, 922–926.
41 C. Zeng, Y. Chen, K. Kirschbaum, K. J. Lambright and R. Jin, *Science*, 2016, **354**, 1580–1584.
42 T. Dainese, M. Agrachev, S. Antonello, D. Badocco, D. M. Black, A. Fortunelli, J. A. Gascon, M. Stener, A. Venzo, R. L. Whetten and F. Maran, *Chem. Sci.*, 2018, **9**, 8796–8805.
43 T. Higaki, M. Zhou, K. J. Lambright, K. Kirschbaum, M. Y. Sfeir and R. Jin, *J. Am. Chem. Soc.*, 2018, **140**, 5691–5695.
44 S. Zhuang, L. Liao, Y. Zhao, J. Yuan, C. Yao, X. Liu, J. Li, H. Deng, J. Yang and Z. Wu, *Chem. Sci.*, 2018, **9**, 2437–2442.
45 C. Zeng, C. Liu, Y. Chen, N. L. Rosi and R. Jin, *J. Am. Chem. Soc.*, 2016, **138**, 8710–8713.
46 Z.-J. Guan, J.-L. Zeng, Z.-A. Nan, X.-K. Wan, Y.-M. Lin and Q.-M. Wang, *Sci. Adv.*, 2016, **2**, e1600323.
47 K. Konishi, M. Iwasaki, M. Sugiuchi and Y. Shichibu, *J. Phys. Chem. Lett.*, 2016, **7**, 4267–4274.
48 Y. Niihori, S. Hossain, S. Sharma, B. Kumar, W. Kurashige and Y. Negishi, *Chem. Rec.*, 2017, **17**, 473–484.
49 C. Zeng, T. Li, A. Das, N. L. Rosi and R. Jin, *J. Am. Chem. Soc.*, 2013, **135**, 10011–10013.
50 Y. Chen, C. Zeng, D. R. Kauffman and R. Jin, *Nano Lett.*, 2015, **15**, 3603–3609.
51 C. Zeng, Y. Chen, C. Liu, K. Nobusada, N. L. Rosi and R. Jin, *Sci. Adv.*, 2015, **1**, e1500425.
52 Y. Chen, C. Liu, Q. Tang, C. Zeng, T. Higaki, A. Das, D.-e. Jiang, N. L. Rosi and R. Jin, *J. Am. Chem. Soc.*, 2016, **138**, 1482–1485.
53 Y. Chen, C. Zeng, C. Liu, K. Kirschbaum, C. Gayathri, R. R. Gil, N. L. Rosi and R. Jin, *J. Am. Chem. Soc.*, 2015, **137**, 10076–10079.
54 C. Zeng, Y. Chen, K. Kirschbaum, K. Appavoo, M. Y. Sfeir and R. Jin, *Sci. Adv.*, 2015, **1**, e1500045.
55 A. Dass, S. Theivendran, P. R. Nimmala, C. Kumara, V. R. Jupally, A. Fortunelli, L. Sementa, G. Barcaro, X. Zuo and B. C. Noll, *J. Am. Chem. Soc.*, 2015, **137**, 4610–4613.
56 J. Zheng, C. Zhou, M. Yu and J. Liu, *Nanoscale*, 2012, **4**, 4073–4083.
57 M. S. Devadas, J. Kim, E. Sinn, D. Lee, T. Goodson III and G. Ramakrishna, *J. Phys. Chem. C*, 2010, **114**, 22417–22423.
58 M. S. Devadas, V. D. Thanthirige, S. Bairu, E. Sinn and G. Ramakrishna, *J. Phys. Chem. C*, 2013, **117**, 23155–23161.
59 H. Qian, M. Y. Sfeir and R. Jin, *J. Phys. Chem. C*, 2010, **114**, 19935–19940.
60 T. D. Green and K. L. Knappenberger, *Nanoscale*, 2012, **4**, 4111–4118.
61 T. D. Green, C. Yi, C. Zeng, R. Jin, S. McGill and K. L. Knappenberger, *J. Phys. Chem. A*, 2014, **118**, 10611–10621.
62 C. Zeng, Y. Chen, K. Iida, K. Nobusada, K. Kirschbaum, K. J. Lambright and R. Jin, *J. Am. Chem. Soc.*, 2016, **138**, 3950–3953.
63 D. M. Chevrier, C. Zeng, R. Jin, A. Chatt and P. Zhang, *J. Phys. Chem. C*, 2015, **119**, 1217–1223.
64 S. Knoppe, S. Malola, L. Lehtovaara, T. Bürgi and H. Häkkinen, *J. Phys. Chem. A*, 2013, **117**, 10526–10533.
65 W. W. Xu, B. Zhu, X. C. Zeng and Y. Gao, *Nat. Commun.*, 2016, **7**, 13574.
66 Z. Ma, P. Wang and Y. Pei, *Nanoscale*, 2016, **8**, 17044–17054.
67 L. Liu, J. Yuan, L. Cheng and J. Yang, *Nanoscale*, 2017, **9**, 856–861.
68 T. Higaki, C. Liu, Y. Chen, S. Zhao, C. Zeng, R. Jin, S. Wang, N. L. Rosi and R. Jin, *J. Phys. Chem. Lett.*, 2017, **8**, 866–870.
69 M. Zhou, S. Tian, C. Zeng, M. Y. Sfeir, Z. Wu and R. Jin, *J. Phys. Chem. C*, 2017, **121**, 10686–10693.
70 V. W. Yam, V. K. Au and S. Y. Leung, *Chem. Rev.*, 2015, **115**, 7589–7728.
71 C. Lavenn, N. Guillou, M. Monge, D. Podbevšek, G. Ledoux, A. Fateevae and A. Demessence, *Chem. Commun.*, 2016, **52**, 9063–9066.
72 C. Zeng, M. Zhou, C. Gayathri, R. R. Gil, M. Y. Sfeir and R. Jin, *Chin. J. Chem. Phys.*, 2018, **31**, 555.